Two-color stabilization of atomic hydrogen in circularly polarized laser fields

D. Bauer*

Theoretische Quantenphysik & Theoretische Quantenelektronik, Institut für Angewandte Physik, Technische Universität Darmstadt, Hochschulstrasse 4a, 64289 Darmstadt, Germany

F. Ceccherini

Dipartimento di Fisica "Enrico Fermi," Università di Pisa & INFM, sezione A, Via Buonarroti 2, 56127 Pisa, Italy

The dynamic stabilization of atomic hydrogen against ionization in high-frequency single- and two-color, circularly polarized laser pulses is observed by numerically solving the three-dimensional, time-dependent Schrödinger equation. The single-color case is revisited and numerically determined ionization rates are compared with both, the exact and the approximate high-frequency Floquet rates. The positions of the peaks in the photoelectron spectra can be explained with the help of dressed initial states. In two-color laser fields of opposite circular polarization, the stabilized probability density may be shaped in various ways. For laser frequencies ω_1 and $\omega_2 = n\omega_1$, $n = 2,3,\ldots$, and sufficiently large excursion amplitudes, $(n+1)$ distinct probability density peaks are observed. This may be viewed as the generalization of the well-known "dichotomy" in linearly polarized laser fields, i.e, as "trichotomy," "quatrochotomy," "pentachotomy" etc. All those observed structures and their "hula-hoop"-like dynamics can be understood with the help of high-frequency Floquet theory and the two-color Kramers-Henneberger transformation. The shaping of the probability density in the stabilization regime can be realized without additional loss in the survival probability, as compared to the corresponding single-color results.

I. INTRODUCTION

For sufficiently high laser frequency and intensity, the ionization probability of an atom decreases by further increasing the laser intensity. This, at first sight, counterintuitive effect is called dynamic or adiabatic stabilization, depending on the pulse length [1–8]. So far, it has been observed in numerical simulations only (see Ref. [9] and, for very recent results, Refs. [10,11]). Its theoretical explanation is most elucidating in the framework of high-frequency Floquet theory [4]: the time-averaged Kramers-Henneberger potential, as it is seen by a free electron moving in the laser field, provides bound states. The electronic probability density of these states is spread over the spatial regions with dimensions of the order of the classical excursion amplitude which may be tens of atomic units or more. The laser frequency ω, required for dynamic stabilization where the electron starts from the field-free ground state with binding energy $\mathcal{E}_0$, has to exceed the field-dressed binding energy, $\hbar\omega > |\mathcal{E}_0'|$. Since such high frequencies are not yet accessible to nowadays intense laser systems, the experimental verification of the dynamic stabilization is still to come. However, with the intense, short wavelength, and coherent light sources under construction worldwide (e.g., at DESY in Hamburg), ground-state stabilization should become experimentally accessible soon. Signatures of the dynamic stabilization of Rydberg atoms, where $|\mathcal{E}_0'|$ is smaller, have been measured [12].

The dynamic stabilization has been studied extensively during the last decade. The ionization rates and energy shifts were obtained numerically by the Floquet theory [13] or approximate, analytical high-frequency Floquet theory [2,4]. Full numerical *ab initio* solutions of the time-dependent single-electron Schrödinger equation were obtained for the low-dimensional model systems (see, e.g., Refs. [14–19]) and, after the early work in Ref. [9] very recently, in three spatial dimensions for linear polarization [10] and circularly polarized laser pulses [11]. Although the Floquet ionization *rates* decrease monotonically for laser intensity $I \to \infty$, the ionization *probability* in full *ab initio* solutions of the time-dependent Schrödinger equation (TDSE) for *finite* laser pulses assumes a minimum and increases again thereafter. In the limit of laser intensity $I \to \infty$ but otherwise fixed pulse parameters, the survival probability of an atom will thus approach zero. Moreover, it has been found that the magnetic field of the laser—usually neglected because of the dipole approximation—leads to increased ionization [20]. This is due to the ponderomotive force that pushes the electrons in the propagation direction. In multielectron atoms, electron correlation also hinders stabilization (see Ref. [21], and references therein). The two-color interference effects on stabilization in linear polarization was studied in Ref. [22,23].

In this paper, the dynamic stabilization of H in circularly polarized single- and two-color fields is investigated. The paper is organized as follows: in Sec. II, the three-dimensional time-dependent Schrödinger equation to be solved numerically is introduced, and the form of the applied two-color fields is explained. In Sec. III, the results concerning the single-color circular polarization case are presented. Besides snapshots of the probability density and the photoelectron spectra, particular emphasis is put on the comparison of ionization rates and energy shifts with results from Floquet theory. In Sec. IV, the main two-color results are

*Email address: dieter.bauer@physik.tu-darmstadt.de

presented. The probability density structures are observed which display well-separated maxima, the number of which is related to the frequency ratio of the two fields. The structure moves as a whole in the laser field and can be explained with the help of the two-color time-averaged Kramers-Henneberger potentials. The survival probabilities after the two-color pulses are presented as a function of the two laser's peak field strengths. The two-color survival probabilities and above-threshold ionization spectra are compared with the corresponding single-color results where the second field was absent. It is good news that adding a second color is possible without a drastic inhibition of stabilization even if the second laser's intensity lies in the "Death Valley" of high ionization. Finally, we conclude in Sec. V.

II. THEORY

The TDSE for the electron of atomic hydrogen in the electric field of a laser,

$$i\frac{\partial}{\partial t}\Psi(\boldsymbol{r},t) = \left(\frac{1}{2}[-i\boldsymbol{\nabla}+\boldsymbol{A}(t)]^2 - \frac{1}{r}\right)\Psi(\boldsymbol{r},t), \qquad (1)$$

is solved numerically in three spatial dimensions (atomic units are used unless noted otherwise). The intense laser field can be treated classically. Since the laser wavelength is large compared to all other relevant length scales and the electron dynamics is nonrelativistic for our laser parameters, the dipole approximation can be applied so that the vector potential $\boldsymbol{A}(t)$ does not depend on the spatial coordinates. Hence, the magnetic component of the laser field is neglected. If we restrict ourselves to study the *coplanar* two-color fields (of, however, arbitrary ellipticity), we may choose the coordinate system in such a way that the z component of the electric field $\boldsymbol{E}(t) = -\partial_t\boldsymbol{A}(t)$ vanishes:

$$\boldsymbol{E}(t) = \boldsymbol{E}^{(1)}(t) + \boldsymbol{E}^{(2)}(t) = [E_x^{(1)}(t) + E_x^{(2)}(t)]\boldsymbol{e}_x$$
$$+ [E_y^{(1)}(t) + E_y^{(2)}(t)]\boldsymbol{e}_y. \qquad (2)$$

The wave function $\Psi(\boldsymbol{r},t)$ is expanded in spherical harmonics,

$$\Psi(r,\vartheta,\varphi,t) = \frac{1}{r}\sum_{\ell=0}^{\infty}\sum_{m=-\ell}^{\ell}\Phi_{\ell m}(r,t)Y_{\ell m}(\vartheta,\varphi),$$

which leads to a set of coupled TDSEs for the radial wave functions $\Phi_{\ell m}(r,t)$,

$$i\frac{\partial}{\partial t}\Phi_{\ell m}(r,t) = \left(-\frac{1}{2}\frac{\partial^2}{\partial r^2} + V_\ell^{\mathrm{eff}}(r)\right)\Phi_{\ell m}(r,t) + i\sqrt{\frac{2\pi}{3}}\sum_{\ell'm'}\left\{\widetilde{A}^*(t)\langle\ell m|11|\ell'm'\rangle\frac{\partial}{\partial r} - \widetilde{A}(t)\langle\ell m|1-1|\ell'm'\rangle\frac{\partial}{\partial r}\right.$$

$$-\frac{\widetilde{A}^*(t)}{r}\langle\ell m|11|\ell'm'\rangle(1+m') + \frac{\widetilde{A}(t)}{r}\langle\ell m|1-1|\ell'm'\rangle(1-m') - \frac{\widetilde{A}^*(t)}{r}\langle\ell m|10|\ell'm'+1\rangle N_{\ell'm'}^+$$

$$\left.+\frac{\widetilde{A}(t)}{r}\langle\ell m|10|\ell'm'-1\rangle N_{\ell'm'}^-\right\}\Phi_{\ell'm'}(r,t), \qquad (3)$$

where $V_\ell^{\mathrm{eff}}(r) = -(1/r) + \ell(\ell+1)/2r^2$ is the effective atomic potential including the centrifugal barrier, $\widetilde{A}(t) = A_x(t) + iA_y(t)$, $N_{\ell m}^\pm = \sqrt{(\ell\mp m)(\ell\pm m+1)/2}$, and the purely time-dependent A^2 term has been transformed away. The matrix elements $\langle\ell m|LM|\ell'm'\rangle := \int d(\cos\vartheta)\,d\varphi\,Y_{\ell m}^*(\vartheta,\varphi)Y_{LM}(\vartheta,\varphi)Y_{\ell'm'}(\vartheta,\varphi)$ may be expressed in terms of Clebsch-Gordan coefficients.

It is worth noticing the coupling of different ℓ and m quantum numbers in the TDSE (3) due to the laser field: there is a $\ell m\to\ell\pm1,m\pm1$ coupling as well as a $\ell m\to\ell\mp1,m\pm1$ coupling (where compatible with the condition $-\ell\leq m\leq\ell$). From the knowledge of these couplings, one can immediately deduce nonperturbative selection rules, e.g., if the initial wave function is the $1s$ ground state, the states with $\ell=1$, $m=0$; with $\ell=2$, $m=\pm1$; with $\ell=3$, $m=\pm2$ etc., are "unreachable" and thus remain unoccupied.

In the actual implementation, the radial coordinate r was discretized directly in position space. The details of the

implementation may be found in Ref. [24] and is similar to what has been described in Ref. [25] for the simpler case of linear polarization.

The radius of our numerical grid, including the region where the nonvanishing imaginary potential damps away the probability density approaching the grid boundary, was between 240 a.u. and 450 a.u. The maximum ℓ quantum number was typically $\ell_{\mathrm{max}}=30$. For testing the convergence of our results, runs up to $\ell_{\mathrm{max}}=50$ were also performed—with no significant changes in the observables of interest. For obtaining the results presented in this paper, the run times of our Schrödinger solver were always less than 18 h on 1-GHz PCs.

We focus on the two-color fields where the both fields are circularly polarized. We assume a $\sin^2$-shaped up and down ramp of the ith field, $i=1,2$ over $N_1^{(i)}=N_{23}^{(i)}$ cycles and a constant part of $N_{12}^{(i)}$ cycles duration. In the following, we will refer to such a pulse as a $(N_1^{(i)},N_{12}^{(i)},N_{23}^{(i)})$ pulse. For the ith electric field in, say, x direction

$$E_x^{(i)}(t)=\begin{cases} E_{ud}^{(i)}(t) & \text{for} & 0\leq t<T_1, \\ \hat{E}^{(i)}\cos\omega_i t & \text{for} & T_1\leq t<T_2, \\ E_{ud}^{(i)}(t-T_2+T_1) & \text{for} & T_2\leq t<T_3, \\ 0, & \text{otherwise} & \end{cases}$$

(4)

is set where $E_{ud}^{(i)}(t)=\hat{E}^{(i)}\sin^2(\pi t/2T_1)\cos\omega_i t$. The absolute ramping time as well as the duration of the constant part of the laser pulse are chosen the same for both colors so that the times $T_1=2\pi N_1^{(i)}/\omega_i$, $T_2=T_1+2\pi N_{12}^{(i)}/\omega_i$, etc., are independent of i. Since we are interested in *opposite* circular polarizations,

$$E_y^{(1)}(t)=E_x^{(1)}(t-3\pi/2\omega_1), \quad E_y^{(2)}(t)=E_x^{(2)}(t-\pi/2\omega_2)$$

(5)

are taken as the y components of the two colors. The corresponding vector potential can be calculated from $A(t)=-\int_0^t dt' E(t')$. In such two-color pulses, as long as $N_1^{(i)}=N_{23}^{(i)}$, $N_{12}^{(i)}$ are integer numbers, a *free* electron (initially at rest) returns to its starting point at the end of the laser pulse—without residual drift momentum.

III. THE CIRCULAR SINGLE-COLOR CASE REVISITED

Before turning to the two-color study, let us analyze the simpler single-color case. For the latter, results from *ab initio* solutions of the three-dimensional TDSE were obtained only recently [10], whereas two-dimensional model solutions were presented earlier [16–19]. The ionization *rates* as well as energy shifts for hydrogen in the stabilization regime (with dipole approximation) are available for several years [13], so that a comparison with our finite pulse results is possible and will be presented in this paper. Since all vector potential amplitudes $\hat{A}$ considered in this work are ≤ 10 a.u., the dipole approximation is applicable, as has been shown in Ref. [20].

A. Survival probability vs time

In order to calculate the probability for the hydrogen atom to "survive" nonionized till the end of the pulse, the probability density is integrated over a spherical volume of radius $R_b=60$ a.u.. The radius R_b was chosen several times greater than the biggest excursion amplitude $\hat{\alpha}=10$ a.u. considered in this paper. Since the free part of the wave function vanishes inside that sphere at sufficiently large times after the laser pulse has passed by, the amount of probability density inside the sphere leads then with high accuracy to the same probability that one would obtain by projecting on all bound states. The results are presented in Fig. 1. In Fig. 1(a), the results for $\omega=1$ are presented, in Fig. 1(b) those for $\omega=2$. All pulses were up and down ramped over four cycles. The constant part of the pulse lasted 16 cycles for $\omega=1$ and 32 cycles for $\omega=2$. From Fig. 1, the very existence of dynamic stabilization is proven: the survival probability at the end of the pulse increases with increasing peak field strength (attached to the curves) up to a maximum value. Increasing the
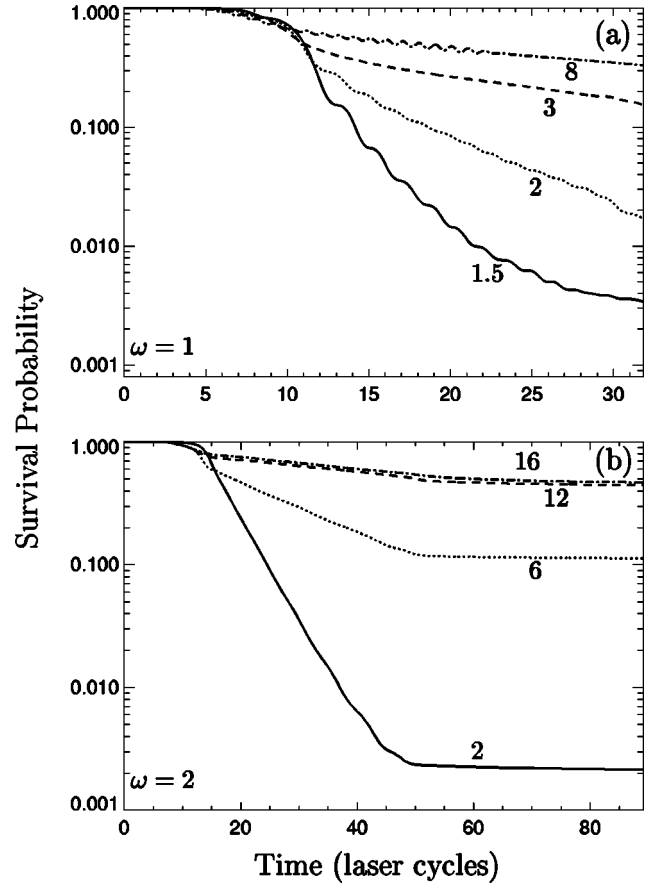
FIG. 1. The probability density, integrated over a sphere of radius $R_b=60$ for laser pulses of frequency $\omega=1$ (a) and $\omega=2$ (b) vs time. (4,16,4) and (4,32,4) pulses were chosen for $\omega=1$ and $\omega=2$, respectively. The $\hat{E}$ values are attached to the curves. The survival probability increases with increasing peak field strengths, but not beyond a certain maximum. In some of the cases, an ionization rate can be determined from the (in the logarithmic plot) linear slope.

peak field strength further yields a decreasing survival probability (not shown in Fig. 1). The highest survival probability in Fig. 1(b) amounts to $\approx 47\%$. It should be noted, however, that the survival probability is rather sensitive to the laser pulse shape and duration. This was also found in the case of linear polarization and is discussed at length in Ref. [10].

Whenever the slope of the probability curves vs time is linear on the logarithmic scale, an ionization *rate* can be determined. While this is straightforward for the curves in the $\omega=2$ panel, it turns out to be more difficult for the $\omega=1$ results in Fig. 1(a). Longer pulses of constant intensity are then needed to obtain unambiguous rates.

B. Snapshots of the probability density

For sufficiently large excursions $\hat{\alpha}$ and adiabatic turn ons, one expects the system to occupy essentially the ground state in the time-averaged Kramers-Henneberger (KH) potential. This corresponds to lowest-order high-frequency Floquet theory [4]. The KH potential is the ionic potential a free
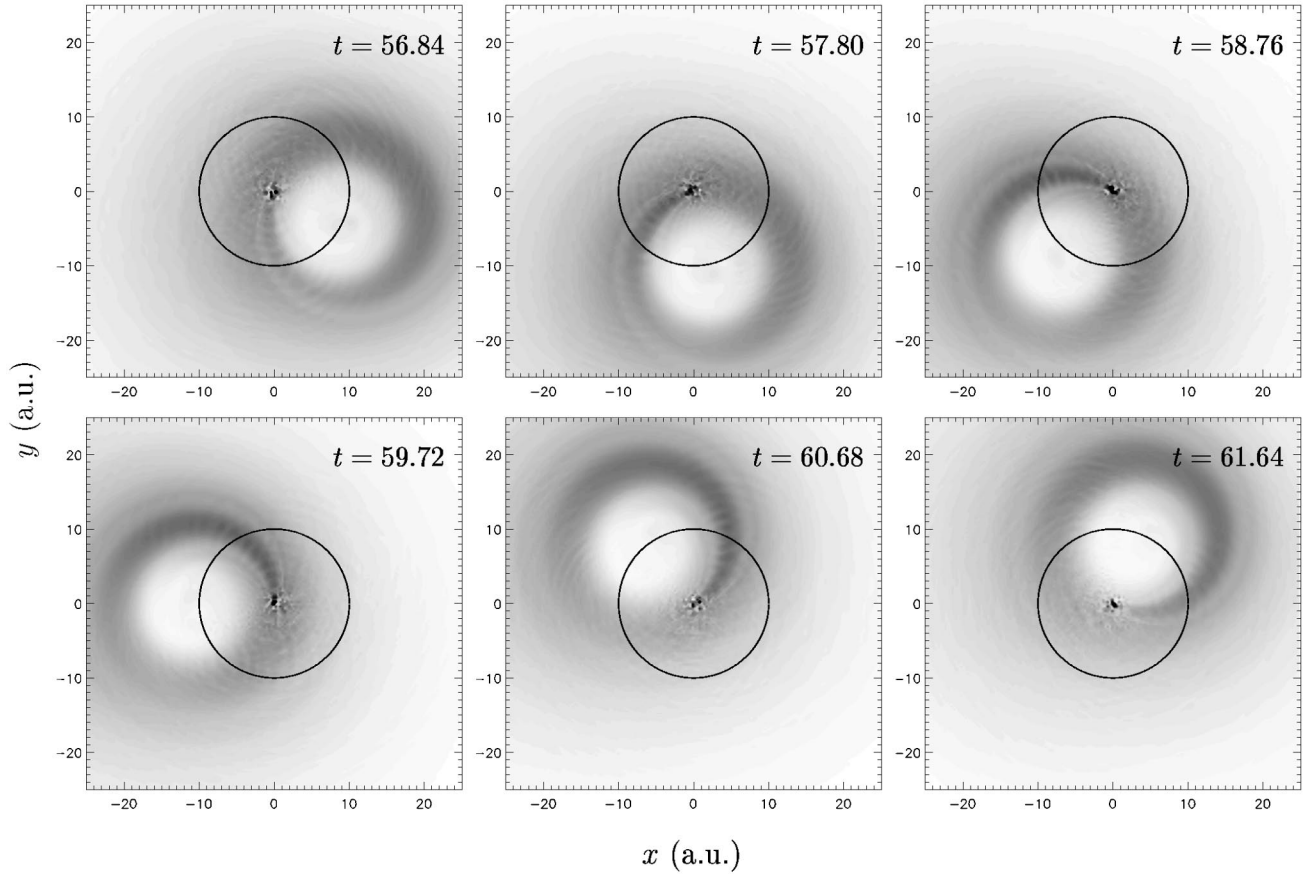
FIG. 2. Series of contour plots of the probability density in the x-y plane at $z=0$ during the ninth cycle of the (2,8,2) laser pulse for $\omega_1=1$ and $\hat{E}_1=10$. The color coding of the probability density is linear. The overlaid black circle of radius $\hat{\alpha}=10$ indicates the corresponding free-electron trajectory. A clockwise ''hula-hoop''-like [11] dynamics of the probability density ring is observed.

electron, just oscillating in the laser field, would ''see,'' i.e., $V_{KH}(\mathbf{r})=V(\mathbf{r}+\boldsymbol{\alpha}(t))$, where $\boldsymbol{\alpha}(t)$ is the trajectory of a free electron in the field,

$$\boldsymbol{\alpha}(t)=\int_0^t dt' \, \mathbf{A}(t'). \quad (6)$$

In the case of a single-color circularly polarized laser, the KH potential, averaged over one laser cycle, has azimuthal symmetry with respect to the laser propagation direction (the z axis in our case) and, for sufficiently big $\hat{\alpha}$, its minimum along a circle of approximate radius $\hat{\alpha}$ in a plane perpendicular to it (the x-y plane in our case). Consequently, the KH ground-state probability density has its maximum along that circle. By transforming back to the lab frame, where the ionic potential is assumed centered at the origin, this ring-shaped stabilized probability density orbits with its center along the free-electron trajectory which itself is a circle of radius $\hat{\alpha}$. What results is a ''hula-hoop''-like dynamics [11] of a probability density ring about the ion that assumes the role of the ''hula-hoop''-dancer's hip.

In Fig. 2, we present snaphots of the probability density in the x-y plane at $z=0$ during the ninth laser cycle of the (2,8,2) pulse with $\omega=1$. The peak field strength was $\hat{E}$

$=10$, yielding an excursion radius $\hat{\alpha}=10$. Although a probability density ring, describing the previously explained ''hula-hoop'' dynamics, is clearly visible, the probability density is not uniformly distributed along that ring but has rather a sicklelike shape. Hence, the system is obviously not in the KH ground state but in a superposition of states with different azimuthal quantum numbers. This leads to Rabi oscillations on time scales that are large compared to the laser period. Note that there is always a probability density maximum at the position of the ion. For lower values of $\hat{\alpha}$, we observed more complex situations where no clear ring structure but two or more wave packets swirl about the ion.

C. Ionization rates

For the single-color case, accurate ionization rates were numerically obtained many years ago by means of nonperturbative Floquet theory [13]. Those rates are accurate in the sense that *if* the system somehow manages to occupy a single Floquet state, it will decay precisely with the corresponding Floquet rate. Usually an adiabatic turn on is needed to transfer the system from the field-free ground state to a single Floquet state. The problem is that an adiabatic ramping of the laser pulse counteracts stabilization because the system has to spend too much time in the so-called ''death valley''
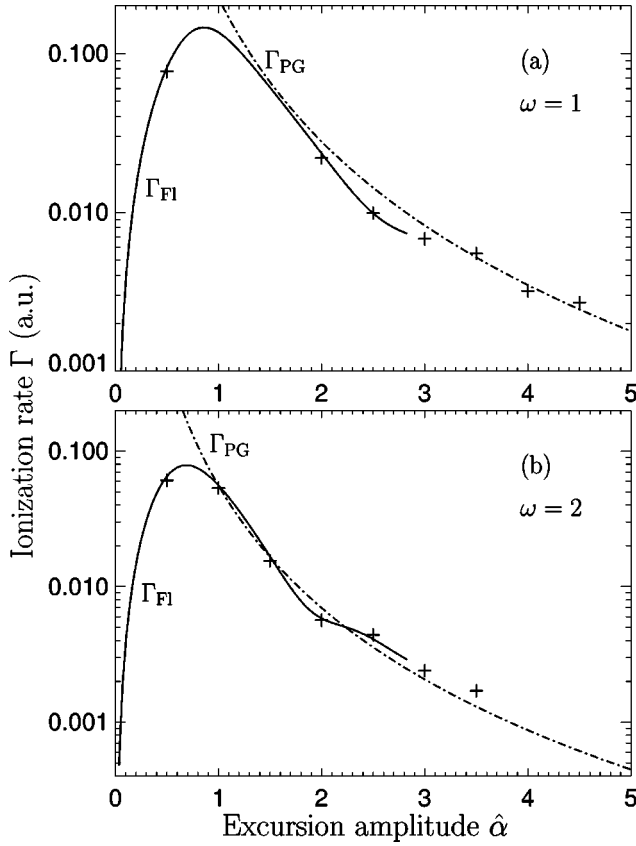
FIG. 3. Ionization rates vs excursion amplitude $\hat{\alpha}$ for (a) $\omega=1$ and (b) $\omega=2$ a.u. Our numerical results ($+$), the full Floquet rates Γ_{Fl} from Ref. [13] (solid), and the analytical result by Pont and Gavrila [2,4] Γ_{PG} (dashed-dotted) are shown.

of medium laser intensities where the ionization is strong, and thus nothing would survive to be stabilized. Hence, short turn-on times are desirable. However, after such rapid turn ons the system might be "shaken up" into a superposition of many Floquet states. Under such conditions only the full solution of the TDSE yields reliable ionization probabilities and, if existing, ionization rates.

In Fig. 3, our ionization rates for $\omega=1$ and $\omega=2$ (determined from plots such as those in Fig. 1) are compared with Floquet results [13] and the analytical results derived by Pont and Gavrila [2,4]. The Pont-Gavrila rate for circular polarization,

$$\Gamma_{\mathrm{PG}} \approx \frac{0.223}{\hat{\alpha}^4 \omega^2}, \qquad (7)$$

was derived from high-frequency Floquet theory combined with the first-order Born approximation. In order to meet the plane-wave criterion of the Born approximation, the excursion amplitude $\hat{\alpha}$ must not be too small. For high frequencies and $\hat{\alpha} \gg 1$, the Pont-Gavrila rate should merge with the full Floquet result. However, in Ref. [13] Floquet rates were calculated only for moderate values of $\hat{\alpha}$ [note, that, by definition, the excursion amplitude $\hat{\alpha}$ for circular polarization in Ref. [13] differs by a factor of $\sqrt{2}$ with Pont and Gavrila's,
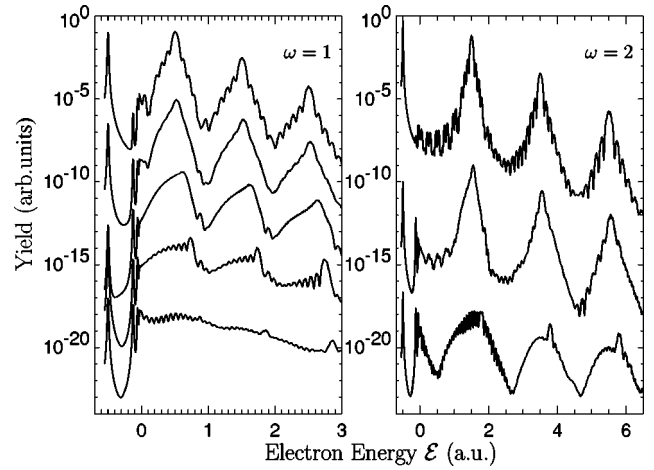
FIG. 4. ATI photoelectron spectra for $\omega=1$ (left panel) and $\omega=2$ (right panel) after (4,8,4) pulses (for $\omega=1$) and (8,16,8) pulses (for $\omega=2$). For clarity, the spectra are shifted vertically with respect to each other. The peak field strengths were (left panel, from top to bottom) $\hat{E}=0.3,0.5,1,2,5$ a.u. and (right panel, from top to bottom) $\hat{E}=0.6,2,10$ a.u. For certain laser intensities, excited states come into play, leading to pronounced modulations of the ATI peaks. With increasing laser intensity, the ATI peaks move towards higher energies.

and ours, i.e., $\Gamma_{\mathrm{PG}}=\Gamma_{\mathrm{Fl}}/\sqrt{2}$]. For $\omega=2$, the Pont-Gavrila rate comes close to the full Floquet result already for $\hat{\alpha}=1$. By increasing $\hat{\alpha}$, the full Floquet result oscillates around the Gavrila rate. In the lower frequency case $\omega=1$, the Gavrila rate overestimates ionization. Our numerical rates were obtained from simulations of (4,16,4) pulses for $\omega=1$ and (4,32,4) pulses for $\omega=2$. The results for the highest $\hat{\alpha}$ values shown were difficult to determine because the ionization probability curves vs time displayed no clear exponential decrease. In order to determine unambiguous ionization rates also for higher $\hat{\alpha}$, a more adiabatic up ramp of the laser field and a longer pulse duration would be required. However, since it is not the goal of this paper to determine rates that are probably easier to obtain via Floquet theory, we do not proceed further in this direction. Our numerical results agree well with the full Floquet rates, where available. For $\omega=1$ and $\hat{\alpha} \gtrsim 3.5$, the Gavrila rate agrees quite well with our numerical data, whereas for $\omega=2$ it underestimates ionization.

D. Above-threshold ionization (ATI)

In Fig. 4, the photoelectron spectra after (4,8,4) pulses (for $\omega=1$) and (8,16,8) pulses (for $\omega=2$) of different peak field strength are presented. They were calculated from the wave function immediately after the pulse with the window-operator method proposed in Ref. [26]. The three lowest-order ATI peaks $n=1,2,3$, separated by $\hbar\omega$, are clearly visible although they broaden with increasing laser intensity. From lowest-order perturbation theory (LOPT), an exponential decrease of the peak heights $\sim \hat{E}^{2n}$ with increasing n is expected. Within high-frequency Floquet theory, for $\hat{\alpha} \gg 1$,
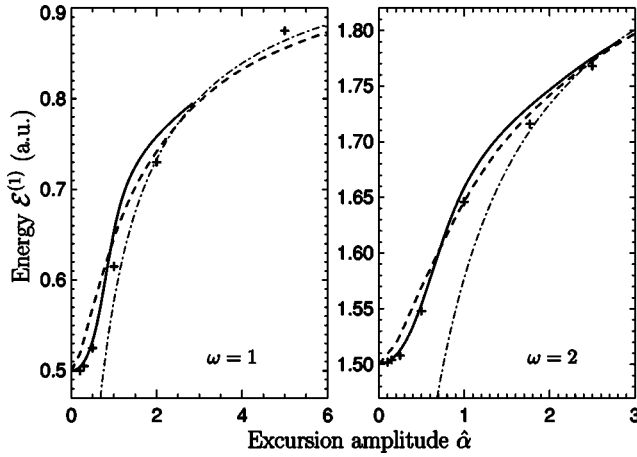
FIG. 5. The energy $\mathcal{E}^{(1)}$ of ATI peak $n=1$ vs the excursion amplitude $\hat{\alpha}=\hat{E}/\omega^2$ for $\omega=1$ (left plot) and $\omega=2$ (right plot). The + symbols are our numerical results. The curves give the expected position of ATI peak $n=1$ according to Eq. (9) with $\mathcal{E}_0'$ from the full Floquet calculation [13] (solid line), with $\mathcal{E}_0'$ as the ground state of the time-averaged KH potential [2] (dashed), and with $\mathcal{E}_0'=-(\ln\hat{\alpha}+2.654\,284)/(2\pi\hat{\alpha})$ [1] (dashed-dotted).

$(\mathcal{E}_0'+n\omega)\hat{\alpha}\gg1$, the contributions of higher orders n do not vanish exponentially but only $\sim n^{-2}$ [2]. By virtue of the first two peaks in the highest-$\hat{E}$ spectra of Fig. 4, this trend of increasing importance of higher-order peaks is confirmed [note that in the numerically obtained wave function after the pulse the ATI peak $n=3$ might be slightly suppressed because of the absorbing boundaries]. With increasing population of the excited states, the left shoulder of the ATI peaks becomes more pronounced. For certain laser intensities a substructure of smaller peaks appears. Since these peaks are separated by the energy difference of $n=2$ and $n=3$ states, that is $\Delta\mathcal{E}=(4^{-1}-9^{-1})/2\approx0.07$, this substructure is likely connected to the population of these states. However, we did not perform yet a detailed study of this substructure. Here we want to focus on the ATI peak *positions*. As can be easily inferred from Fig. 4, the ATI peaks move with increasing laser intensity to higher photoelectron energies. This is contrary to what happens for low frequencies and high intensities. In general, the positions of the ATI peaks follow

$$\mathcal{E}_{\text{low}}^{(n)}=\mathcal{E}_0'-\Delta_{\text{cont}}+n\omega. \qquad (8)$$

Here, $\mathcal{E}_0'=\mathcal{E}_0+\Delta$ is the field-dressed ground-state energy that is ac Stark shifted by Δ compared to the unperturbed ground-state energy $\mathcal{E}_0$ ($=-0.5$ for H), and Δ_{cont} is the energy up shift of the continuum threshold. n is the number of absorbed photons $\geq n_{\min}$, where $n_{\min}$ is the smallest integer that gives $\mathcal{E}_{\text{low}}^{(n_{\min})}>0$. For low frequencies, one has $\Delta_{\text{cont}}=U_p=f(\hat{E}^2/2\omega^2)$, where U_p is the ponderomotive potential, i.e., the time-averaged quiver energy of a free electron in the laser pulse of peak field strength $\hat{E}$. The prefactor f is (for our definition of $\hat{E}$) 1 for circular and 1/2 for linear polarization. Since in the case of long wavelengths the up shift of the continuum threshold by U_p is bigger than the shift Δ of
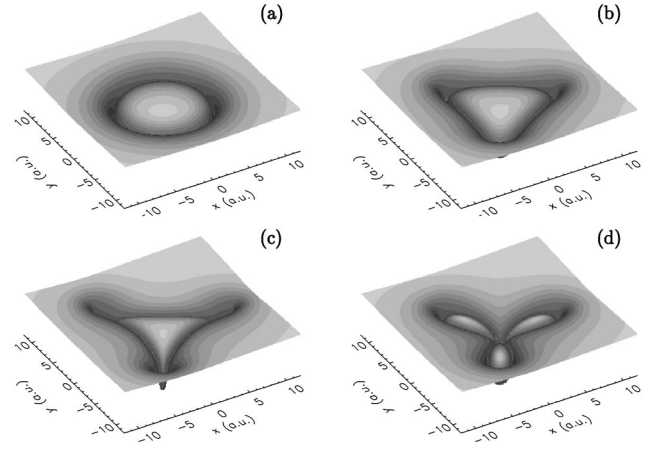
FIG. 6. Time-averaged KH potentials in the x-y plane at $z=0$ for $\omega_1=1$, $\omega_2=2$. The peak field strengths $\hat{E}^{(1)}$, $\hat{E}^{(2)}$ are chosen in such a way that (a) the ω_2 field is absent, $\hat{E}^{(1)}=6$; (b) the two laser intensities are equal, $\hat{E}^{(1)}=\hat{E}^{(2)}=6$; (c) the two vector potential amplitudes are equal, $\hat{E}^{(1)}/\omega_1=\hat{E}^{(2)}/\omega_2=6$; (d) the two excursion amplitudes are equal, $\hat{E}^{(1)}/\omega_1^2=\hat{E}^{(2)}/\omega_2^2=4$. In the two-color cases (b)–(d), the threefold symmetry leads to three minima in the potential. The corresponding KH ground-state probability densities will therefore display "trichotomy," i.e., three spatially separated maxima of the probability density.

the ground state, the ATI peaks move towards lower energies with increasing laser intensities. The "drowning" of a certain peak number n below $\mathcal{E}=0$ is the celebrated "channel closing" in ATI physics.

We shall see that in the stabilization regime, where $\omega>|\mathcal{E}_0'|$ must hold, the shift of ATI peaks is dominated by the ground-state up shift Δ so that

$$\mathcal{E}_{\text{high}}^{(n)}\approx\mathcal{E}_0'+n\omega. \qquad (9)$$

Accurate values of the field-dressed energies $\mathcal{E}_0'$ in the stabilization regime can be obtained from Floquet theory [13]. Solving the set of coupled Floquet equations yields complex energies the real part of which is the field-dressed energy. The complex part is half the ionization rate, $\mathcal{E}_{0,\text{Fl}}=\mathcal{E}_0'-i\Gamma_{\text{Fl}}/2$. From the high-frequency Floquet theory point-of-view, $\mathcal{E}_0'$ is the ground-state energy of the time-averaged KH potential. In Ref. [2], Pont and Gavrila gave KH ground-state energies for H in a circularly polarized laser field. Because $|\mathcal{E}_0'|<|\mathcal{E}_0|$ the ATI peaks move to higher energies with increasing laser intensity—contrary to the high-intensity low-frequency case (8).

In Fig. 5, our numerically determined positions for the $n=1$ ATI peak are compared with Eq. (9), where the value for $\mathcal{E}_0'$ has been determined (i) by the full Floquet solution [13], (ii) as the time-averaged KH potential ground-state energy [2], and (iii) through Pont's approximate formula $\mathcal{E}_0'=-(\ln\hat{\alpha}+2.654\,284)/(2\pi\hat{\alpha})$ [1]. The agreement may be considered acceptable although not excellent. The differences are likely due to the population of more than a single Floquet state. Our numerical result for $\omega=1$ and $\hat{\alpha}=5$ lies above the
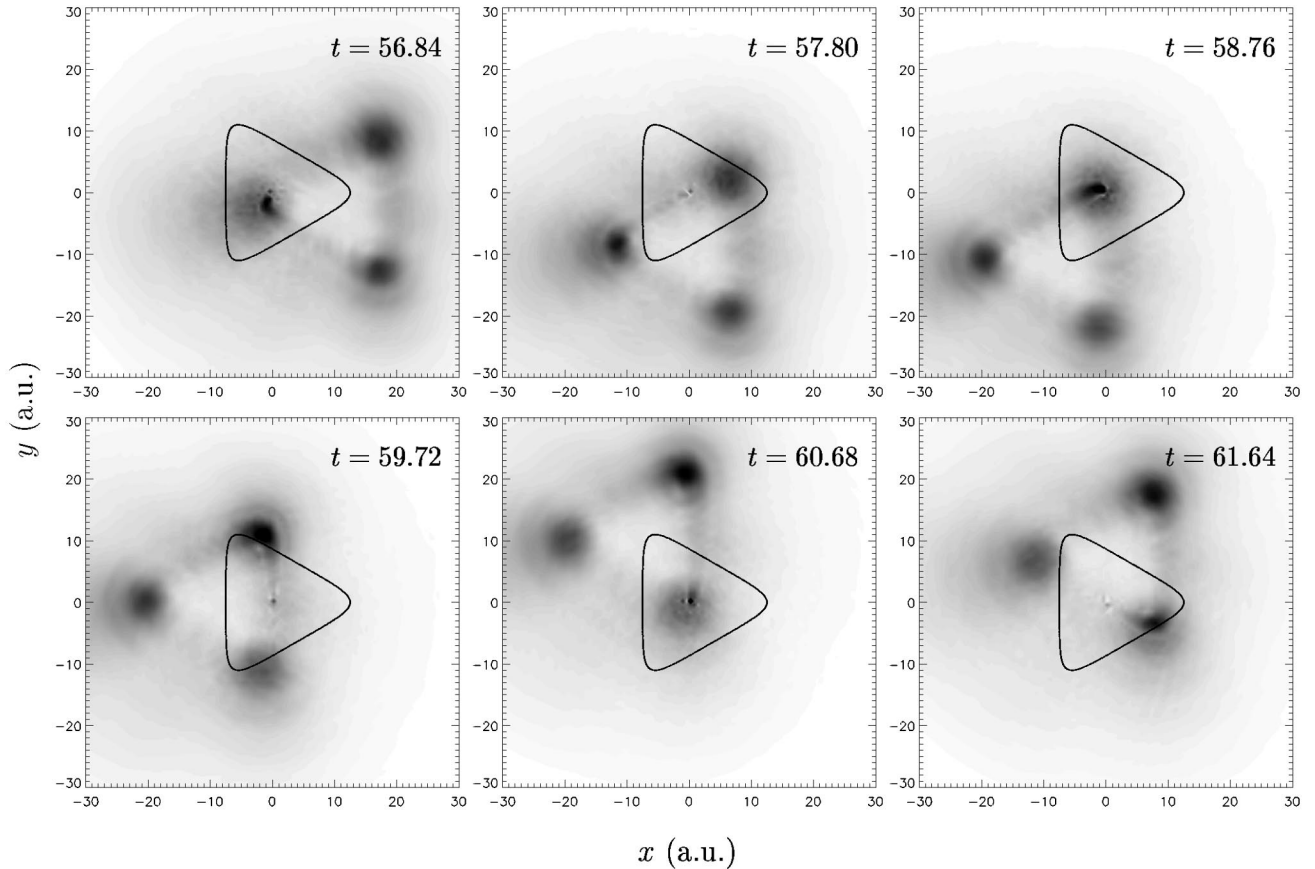
FIG. 7. Series of contour plots of the probability density in the x-y plane at $z=0$ during the ninth (low frequency) cycle of the laser pulse for $\omega_1=1$ [(2,8,2) pulse], $\omega_2=2$ [(4,16,4) pulse], and $\hat{E}_1=\hat{E}_2=10$. "Trichotomy" and "hula-hoop" dynamics are observed, i.e., three peaks of probability density, located in the corners of an equilateral triangle whose center moves along the black triangle, representing the orbit of a free electron in the same laser field. The color coding of the probability density is linear.

analytical curves because the substructure in the ATI spectrum (cf. Fig. 4) also alters the absolute maximum of an ATI peak so that its determination becomes ambiguous.

IV. TWO-COLOR CASE WITH OPPOSITE CIRCULAR POLARIZATIONS

A. Time-averaged KH potentials

It is useful for the analysis of our two-color results to get familiar with the free-electron trajectories in such fields and the corresponding time-averaged KH potentials. In the two-color case, the KH potentials were averaged over the low-frequency laser period $2\pi/\omega_1$. Let us consider the two laser frequencies $\omega_1=1$ and $\omega_2=2$. If the second field is absent, the free-electron trajectory $\boldsymbol{\alpha}(t)$ describes a circle in the x-y plane of radius $\hat{\alpha}_0=\hat{E}^{(1)}/\omega_1^2$. If the second field amplitude $\hat{E}^{(2)}$ equals $\hat{E}^{(1)}$, i.e., both laser fields have the same intensity, the trajectory resembles an equilateral triangle with rounded edges, and $\max|\hat{\alpha}|=5\hat{\alpha}_0/4$. If, instead, the vector potential amplitudes of both fields are equal, $\hat{E}^{(1)}/\omega_1=\hat{E}^{(2)}/\omega_2$, the electron follows a convex triangle with sharp edges, and $\max|\hat{\alpha}|=3\hat{\alpha}_0/2$. Finally, equal excursion amplitudes, i.e., $\hat{E}^{(1)}/\omega_1^2=\hat{E}^{(2)}/\omega_2^2$, yields a rosettelike trajectory,

and $\max|\hat{\alpha}|=2\hat{\alpha}_0$. The time-averaged KH potentials look accordingly. They are presented in Fig. 6. In the two-color cases [Figs. 6(b)–6(d)], the threefold symmetry leads to three potential minima near the turning points. If the stabilized electron occupies the KH ground state, the probability density will show "trichotomy" instead of the well-known "dichotomy" in the case of a single-color linearly polarized laser where two probability peaks, separated by $2\hat{\alpha}$, were observed [9]. In general, when $\omega_2=n\omega_1$ the trajectories display $(n+1)$-fold symmetry. Provided the peak field strengths are properly chosen, for $n=3,4,\ldots,$ the $n+1$ minima of the time-averaged KH potentials will lead to "quatrochotomy," "pentachotomy," etc. The electron dynamics in the laboratory frame should then resemble "hula-hoop" with a triangle, a square, a pentagon, and so forth. We would like to remark that the discrete symmetry of the trajectory and the time-averaged KH potential is closely related to the selection rules for harmonic generation in two-color fields (see Ref. [27], and references therein). If the two fields with frequencies ω_1 and $\omega_2=n\omega_1$ are equally polarized instead of oppositely, the KH potentials have $(n-1)$-fold symmetry. Hence, to obtain "trichotomy" $\omega_2=4\omega_1$ has to be chosen in this case. If the two frequencies are not commensurable, the free-electron trajectories are not closed, and the
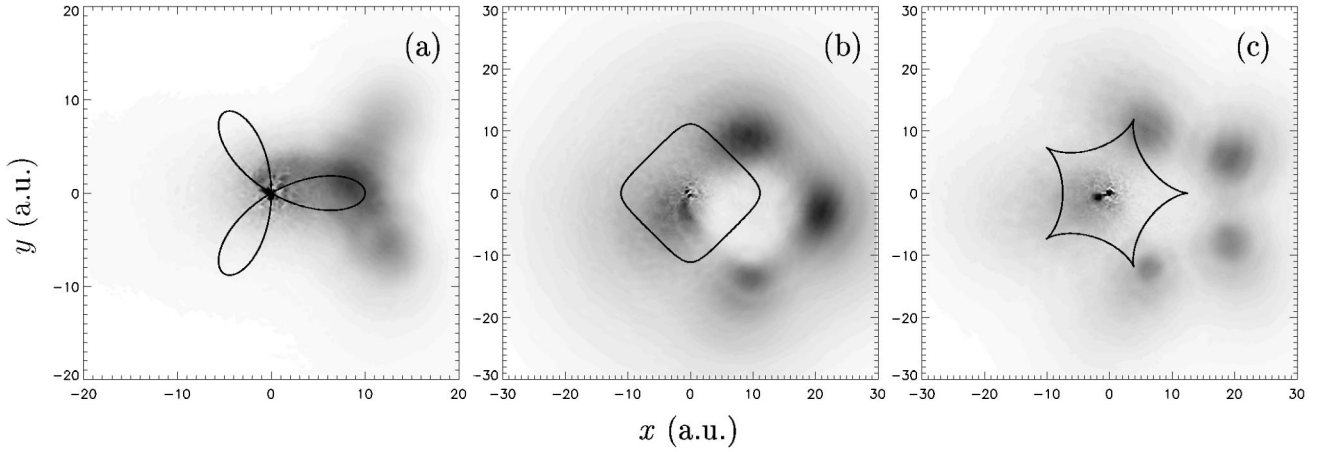
FIG. 8. Probability densities in the x-y plane at $z=0$ and $t=56.84$ during the constant part of a $(2,8,2)$ pulse (with respect to ω_1 $=1$). The second frequency ω_2 was (from left to right) 2, 3, and 4. The laser intensities were chosen such that (a) $\hat{\alpha}^{(1)}=\hat{\alpha}^{(2)}=5$, (b) $\hat{E}^{(1)}=\hat{E}^{(2)}=10$, and (c) $\hat{A}^{(1)}=\hat{A}^{(2)}=10$. The overlaid black curves are the corresponding free-electron trajectories along which the center of the stabilized structure moves.

two-color time-average KH potential is ill defined. However, we observed stabilization also in this case although no distinct probability density peaks were obtained.

B. Snapshots of the probability density

In Fig. 7, snapshots of the trichotomous "hula-hoop" dynamics for $\omega_1=1$, $\omega_2=2$ during one laser cycle (with respect to the $\omega_1=1$ field) is presented. The two laser intensities were chosen equal so that the free-electron trajectory is a triangle with rounded edges. This triangle is drawn in black in each of the plots of Fig. 7. As expected, the center of the trichotomous probability density (aligned along the time-averaged KH potential) moves clockwise along the black triangle. Note that the stabilized structure moves as a whole and does not rotate about its center. In the comoving frame, i.e., the KH frame, the ion swirls along the triangle, forming another probability density maximum. In Fig. 8, three other examples for stabilized probability density are presented. In Fig. 8(a), where the excursion amplitudes for both fields were chosen equal, no three distinct peaks are visible because $\hat{\alpha}=5$ is too small.

In Fig. 8(b), a clear example of equal intensity quatrochotomy (i.e., $\omega_2=3$) is shown, and in Fig. 8(c), a case of pentachotomy ($\omega_2=4$) where both fields had equal vector potential amplitudes. The density of the $n+1$ peaks varies during the course of the laser pulse. This implies that several Floquet states are involved.

C. Survival probability vs time

So far the two-color survival probability was not addressed at all. If, for instance, $\hat{E}^{(2)}$ is chosen so that the $\omega_2=2$ field alone yields optimal stabilization, and a $\omega_1=1$ field with $\hat{E}^{(1)}$ in the "Death Valley" is added—what is the survival probability? In the worst case, ionization would be dominated by the "Death Valley" field, making the two-color stabilization not very attractive. Fortunately, it is not

the field that would lead to highest ionization, if applied alone, it dominates two-color dynamic stabilization. In Fig. 9, the temporal evolution of the survival probability in the two-color case is compared with the two corresponding single-color results. From Fig. 9(a), it is clearly seen that if the two laser intensities are tuned to yield equal excursion amplitudes $\hat{\alpha}$, the two-color survival probability is closer to the single-color high-frequency result with relatively low ionization probability. The low-frequency field alone has a higher ionization probability. In the equal intensity plot [Fig. 9(b)], it is the other way round: the two-color result follows closely the low-frequency curve whereas the high-frequency field alone yields higher ionization because $\hat{E}^{(2)}$ is still close to the "Death Valley." Since in Fig. 9(a) all curves cross each other, it is apparent that the final survival probability is sensitive to the pulse length. However, it should be stressed that, fortunately, the two-color survival probability is *not* determined by the frequency which yields highest ionization. This means that the two-color "probability density shaping," as discussed in the proceding section, can be performed without drastic reduction of the survival probability.

In Fig. 10, the survival probabilities at the end of $(2,8,2)$ and $(4,16,4)$ pulses for $\omega_1=1$ and $\omega_2=2$, respectively, are plotted vs the field amplitudes $\hat{E}^{(1)}$ and $\hat{E}^{(2)}$. Because of the probability density representing free but slow electrons, it takes a long time until the probability density integrated over the sphere of radius $R_b=60$ assumes a constant value. Hence, to obtain Fig. 10 we have chosen to measure the survival probability as the maximum probability to find the electron in a smaller sphere of radius $R_s=7.5$ within a time period of 85 a.u. after the pulse. The maximum probability has to be taken because of the oscillations due to excitation of the $2s$ and the $3s$ state. Note that this method for measuring the survival probability slightly overestimates ionization because the probability density, which represents slow recombining electrons, slowly spirals back to the ion and does not enter the small sphere within the observation time. How-
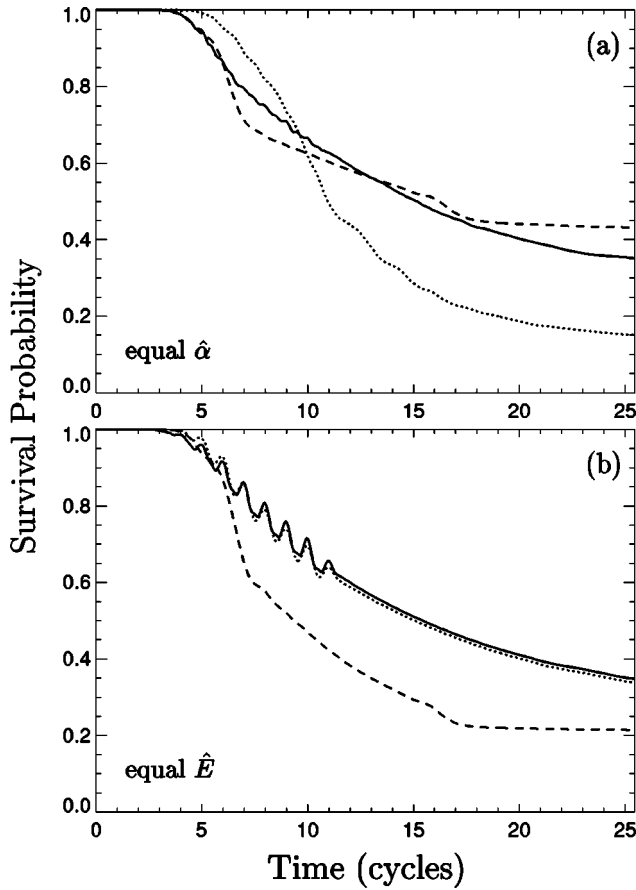
FIG. 9. The survival probability vs time in laser cycles of the lower-frequency field with $\omega_1 = 1$. The full curves are the two-color results for $\omega_2 = 2$, the dotted curves are the results for the low-frequency field alone, the dashed curves are the results for the $\omega_2 = 2$ field alone. In panel (a) the equal excursion amplitude case $\hat{\alpha} = 2$ is shown, while in (b) the equal intensity case $\hat{E} = 6$ is presented. (2,8,2) and (4,16,4) pulses were used for the ω_1 and ω_2 field, respectively.

FIG. 10. The survival probability after a (2,8,2) and (4,16,4) pulse of frequency $\omega_1 = 1$ and $\omega_2 = 2$, respectively, vs the peak field strengths $\hat{E}^{(1)}$ and $\hat{E}^{(2)}$. The data points indicated by vertical lines were calculated, the shaded surface is an interpolation between them. Increasing survival probability for $\hat{E}^{(1)}, \hat{E}^{(2)} \to 0$ was suppressed for the sake of better visibility of the results in the stabilization regime. See text for discussion.

ever, here we are not interested in absolute numbers (which depend sensitively on the pulse duration and shape anyway). From Fig. 10, one infers that the highest survival probability is obtained, as expected, in the single-color high-frequency case where $\hat{E}^{(1)} = 0$. In general, the overall behavior is an increasing stabilization probability up to a maximum value, followed by increasing ionization if the laser intensities are increased further. This is different from high-frequency Floquet theory where the ionization rate monotonically decreases with increasing intensity because the "shake off" during the pulse turn ons and turns offs is not taken into account. In our results, the field strength regime where $\hat{E}^{(1)}/\omega_1, \hat{E}^{(2)}/\omega_2 < 1$ in Fig. 10 may be identified as the "Death Valley" of high ionization probability. Of course, the survival probability increases towards unity as $\hat{E}^{(1)}, \hat{E}^{(2)} \to 0$. However, this has been suppressed in the plot because it blocked the visibility of the results in the stabilization regime in which we are interested. Given a certain $\hat{E}^{(1)}$, adding $\hat{E}^{(2)}$ is, from a stabilization point of view, almost always

beneficial, provided that $\hat{E}^{(2)}$ is not too strong so that shake off dominates. If, on the other hand, we choose a certain $\hat{E}^{(2)}$ and add a ω_1 field, the survival probability may be enhanced or diminished, depending on whether $\hat{E}^{(2)}$ lies in its single-color stabilization regime or near its single-color "Death Valley." The case of a rosettelike stabilized probability density, where the excursion amplitudes $\hat{\alpha}$ are equal, leads only to a relatively small reduction in the survival probability with respect to the optimally stabilized ω_2 field alone (around $\hat{E}^{(2)} = 12$ in Fig. 10). In contrast, the equal intensity result remains close to the low-frequency single-color result where $\hat{E}^{(2)} = 0$. Note that maximum stabilization is achieved for modest values of $\hat{\alpha} = \hat{E}/\omega^2$, where the probability density splitting, i.e., trichotomy, quatrochotomy, etc., is not yet developed.

D. ATI in circular two-color stabilization

Finally, let us briefly discuss the two-color photoelectron spectra. The single-color case has been analyzed in Section III D.

In Fig. 11, the two-color spectra are compared with the corresponding single-color results, where either the $\omega_1 = 1$ field or the $\omega_2 = 2$ field was present. The laser intensities were chosen not deep in the stabilization regime because at such high laser intensities the clear ATI structure gets corrupted by peak broadening and modulations (cf. Fig. 4).

The ATI peaks in the two-color spectra are located at higher energies than those of the corresponding single-color results. This is due to the fact that the ground state in the time-averaged KH potential experiences a stronger up shift as compared to the single-color KH potentials. It would be interesting to analyze the ATI peak positions in the two-color
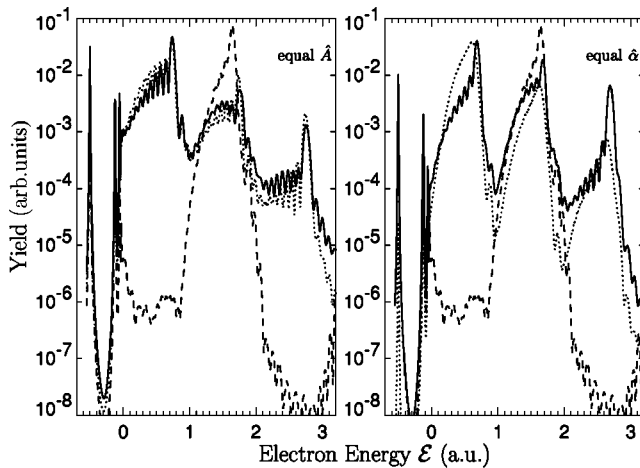
FIG. 11. Comparison of two-color photoelectron spectra (full curve) with the corresponding single-color results, where only the $\omega_1 = 1$ field (dotted) and only the $\omega_2 = 2$ field (broken) were present, respectively. The same pulse shapes as in Fig. 4 were used. The two-color result in the left panel has been obtained with $\hat{A} = \hat{E}^{(1)}/\omega_1 = \hat{E}^{(2)}/\omega_2 = 2$. In the right panel, the excursion amplitudes were equal: $\hat{\alpha} = \hat{E}^{(1)}/\omega_1^2 = \hat{E}^{(2)}/\omega_2^2 = 1$.

case in the same way as it was done in Sec. III D for single-color fields. However, to our knowledge, the two-color Floquet energies for high-frequency circular polarization are not yet published.

As far as the peak strengths are concerned the two-color spectrum is, of course, not simply the sum of the two single-color spectra: the first ATI peak in the single-color ω_2 spectrum is stronger than both the second peak of the two-color and the single-color ω_1 field. This is compatible with Fig. 10 from which one infers that adding to the ω_2 field (whose intensity lies close to the "Death Valley") the lower frequency ω_1 field suppresses ionization. In the equal-$\hat{A}$ result, the two-color spectrum is close to the single-color low-frequency spectrum. Instead, the two-color spectrum for equal $\hat{\alpha}$ is qualitatively different from both two single-color spectra. Not only modulations appear in the two-color result, which are absent in the ω_1 spectrum, but also the height of the peaks differ significantly from each other.

V. CONCLUSION

We have studied the dynamic stabilization of atomic the hydrogen against the ionization in single- and two-color, circularly polarized laser pulses by solving numerically the three-dimensional time-dependent Schrödinger equation. In the single-color case, we confirmed the "hula-hoop"-like dynamics for sufficiently high excursions $\hat{\alpha}$. The ionization rates were compared with those from (high-frequency) Floquet theory, and good agreement was found. The positions of ATI peaks in our numerical photoelectron spectra were analyzed. It was found that the ATI peaks move with increasing laser intensity towards higher energies, in contrast to what happens in intense low-frequency fields. This behavior can be explained by the laser-field-induced up shift of the initially populated field-free ground state.

For two-color laser fields of opposite circular polarization, we presented stabilized probability density structures. For laser frequencies ω_1 and $\omega_2 = n\omega_1$, $n = 2, 3, \ldots$, and sufficiently large excursion amplitudes, $(n+1)$ distinct probability density peaks were observed, in accordance to what one expects by virtue of the two-color time-averaged Kramers-Henneberger potentials. As the generalization of the well-known "dichotomy" in linearly polarized laser fields, we called this multiple probability density peak-splitting trichotomy, quatrochotomy, pentachotomy etc.

The survival probability after two-color pulses of frequencies $\omega_1 = 1$ and $\omega_2 = 2$ was calculated as a function of the two peak field strengths. As expected, highest stabilization is achieved with the high-frequency field alone for a certain optimal laser intensity. However, adding the second low-frequency field, even if its intensity falls into the "Death Valley," fortunately does *not* drastically reduce stabilization, as one might expect from a naive superposition point of view.

[1] M. Pont, Phys. Rev. A **40**, 5659 (1989).

[2] M. Pont and M. Gavrila, Phys. Rev. Lett. **65**, 2362 (1990).

[3] M. Pont, N.R. Walet, and M. Gavrila, Phys. Rev. A **41**, 477 (1990).

[4] Mihai Gavrila, in *Atoms in Intense Laser Fields*, edited by M. Gavrila (Academic Press, San Diego, 1992).

[5] J.H. Eberly and K.C. Kulander, Science **262**, 1229 (1993).

[6] Marvin H. Mittleman, *Introduction to the Theory of Laser-Atom Interactions*, 2nd ed. (Plenum Press, New York 1993).

[7] F.H.M. Faisal, L. Dimou, H.-J. Stiemke, and M. Nurhuda, J. Nonlinear Opt. Phys. Mater. **4**, 701 (1995).

[8] M. Gavrila, in *Multiphoton Processes*, edited by L.F. DiMauro *et al.*, AIP Conf. Proc. 525 (AIP, Melville, NY, 2000).

[9] Kenneth C. Kulander, Kenneth J. Schafer, and Jeffrey L. Krause, Phys. Rev. Lett. **66**, 2601 (1991).

[10] M. Dondera, H.G. Muller, and M. Gavrila, Phys. Rev. A **65**, 031405 (2002).

[11] Dae-Il Choi and Will Chism, Phys. Rev. A **66**, 025401 (2002).

[12] N.J. van Druten, R.C. Constantinescu, L.D. Noordam, and H.G. Muller, Phys. Rev. A **55**, 622 (1997), and references therein.

[13] Martin Dörr, R.M. Potvliege, Daniel Proulx, and Robin Shakeshaft, Phys. Rev. A **43**, 3729 (1991).

[14] Q. Su, J.H. Eberly, and J. Javanainen, Phys. Rev. Lett. **64**, 862 (1990).

[15] E.A. Volkova, A.M. Popov, and O.V. Smirnova, Zh. Éksp.

Teor. Fiz. **106**, 1360 (1994) [JETP **79**, 736 (1994)].

[16] A. Patel, M. Protopapas, D.G. Lappas, and P.L. Knight, Phys. Rev. A **58**, R2652 (1998).

[17] A. Patel, N.J. Kylstra, and P.L. Knight, Opt. Express **4**, 496 (1999); J. Phys. B **32**, 5759 (1999).

[18] Duck-Hee Kwon, Yong-Jin Chun, Hai-Woong Lee, and Yong-joo Rhee, Phys. Rev. A **65**, 055401 (2002).

[19] M. Yu. Ryabikin and A.M. Sergeev, Laser Phys. **12**, 757 (2002).

[20] N.J. Kylstra, R.A. Worthington, A. Patel, P.L. Knight, J.R. Vázquez de Aldana, and L. Roso, Phys. Rev. Lett. **85**, 1835

(2000).

[21] D. Bauer and F. Ceccherini, Phys. Rev. A **60**, 2301 (1999).

[22] Taiwang Cheng, Jie Liu, and Shigang Chen, Phys. Rev. A **59**, 1451 (1999).

[23] R.M. Potvliege, Phys. Rev. A **60**, 1311 (1999).

[24] D. Bauer, Habilitation thesis, TU Darmstadt, 2002 (unpublished).

[25] H.G. Muller, Laser Phys. **9**, 138 (1999).

[26] K.J. Schafer and K.C. Kulander, Phys. Rev. A **42**, 5794 (1990).

[27] F. Ceccherini, D. Bauer, and F. Cornolti, J. Phys. B **34**, 5017 (2001).